



HAL
open science

Modeling Pyrolysis in a High Capacity Thermobalance

Frederic Marias, Stephanie Delage Santacreu

► **To cite this version:**

Frederic Marias, Stephanie Delage Santacreu. Modeling Pyrolysis in a High Capacity Thermobalance. 5th International Conference on Engineering for Waste and Biomass Valorisation, Aug 2014, Rio de Janeiro, Brazil. hal-00996244

HAL Id: hal-00996244

<https://hal.science/hal-00996244>

Submitted on 25 May 2021

HAL is a multi-disciplinary open access archive for the deposit and dissemination of scientific research documents, whether they are published or not. The documents may come from teaching and research institutions in France or abroad, or from public or private research centers.

L'archive ouverte pluridisciplinaire **HAL**, est destinée au dépôt et à la diffusion de documents scientifiques de niveau recherche, publiés ou non, émanant des établissements d'enseignement et de recherche français ou étrangers, des laboratoires publics ou privés.

Modeling Pyrolysis in a High Capacity Thermobalance

F. MARIAS^{1,*} and S.DELAGE²

¹ Laboratoire de Thermique Energétique et Procédés,
Université de Pau et des Pays de l'Adour
Pau, France.

² Laboratoire de Mathématiques et de leurs Applications
Université de Pau et des Pays de l'Adour
Pau, France.

*Corresponding author: frederic.marias@univ-pau.fr.
Telephone 33 559 407 809

Abstract

This work is devoted to the 2D modeling of the transient pyrolysis of biomass in a fixed bed. The model mainly relies on the concept of homogenization of the porous media using the volume averaging theory. This model includes heat and mass transfers in an environment where pyrolysis reactions contribute to the modification of the properties of the media under investigation. This model allows predicting the temperature, moisture, condensable and permanent gases as well as fresh or pyrolysed biomass profiles within the bed. It also allows characterizing the influence of the heat of the pyrolysis reaction on the overall process.

This general model is applied to describe pyrolysis of pine wood particles which are processed in a high capacity thermobalance. A comparison of the experimental and numerical evolution of the mass of the sample during the operation is performed showing very good agreement.

The model is then used to get insights into the weight of the different phenomenon involved in the process on the overall operation.

1- INTRODUCTION

In the frame of the renewal of our energy mix, there is evidence on the fact that biomass is liable to play a major role in the future. Biomass (composed of several compounds) should be either burnt to provide heat, pyrolysed to provide liquid, gas and/or solid fuel, or gasified to produce gas [1-2]. However, both of them involve a pyrolysis step and this step is at the heart of biomass conversion. This work is devoted to the description of this process with an operating temperature below 500°C and heating rates below 20°C/ min (slow pyrolysis).

A mathematical model for the description of this operation occurring in a fixed bed has been developed. It mainly relies on a homogenization procedure using the volume averaging theory [3-4] which allows translating the porous heterogeneous medium under investigation into a continuous one. The pyrolysis reaction is described using a three parallel reaction pathway leading to the formation of a solid residue (char), permanent gases (gas) and gases that might condense at ambient temperature (tars). The results of the model (in terms of overall mass loss of the sample under investigation) are compared upon experimental ones obtained in a high capacity thermobalance.

The first part of the paper is devoted to the description of this experimental device, and to the description of the mathematical model that was developed to represent the different phenomena occurring within this device. In the second part of the paper, the comparison of the results obtained by both methods is performed, and then, some of the results that might be obtained by the model are further developed.

2- MATERIALS AND METHODS

This section is devoted to the presentation of the experimental device and of the mathematical model that were used in the frame of this study.

2.1- High Capacity Thermobalance

The high capacity thermobalance that has been developed at the Laboratoire de Thermique Energétique et Procédés [5-6] operates on the same principle as a commercial TGA. Indeed, thanks to this device, it is possible to record the mass of a sample as a function of its temperature which is controlled by a furnace. Nevertheless, while commercial TGA's can accept loads below 10mg, the high capacity thermobalance is able to process samples up to 1kg. Collecting of the products of the pyrolysis operation is also possible thanks to the apparatus. It is represented on Figure 1.

It is mainly composed of an electrical furnace where batch pyrolysis processes. A basket (PA 101) is used to load the sample under investigation into the furnace. This basket rests on the balance W101 through four "legs" that cross the refractory lining and casing of the furnace (the balance is kept in a cold box, swept by an inert nitrogen flow). Inerting of the furnace and extraction of the gases generated during the operation are achieved thanks to a nitrogen flow that enters the furnace through its bottom and through a distributor that ensure homogeneous velocity profile at the bottom of the sample. This nitrogen flow might be heated up prior entering the furnace thanks to the electrical heater EC101. Gases are withdrawn from the furnace in a heated pipe before entering the condenser EC102 where tars are separated from the gas flow and collected into a storage capacity (BA 101). The resulting gases are then filtered before being analysed and sent to the atmosphere.

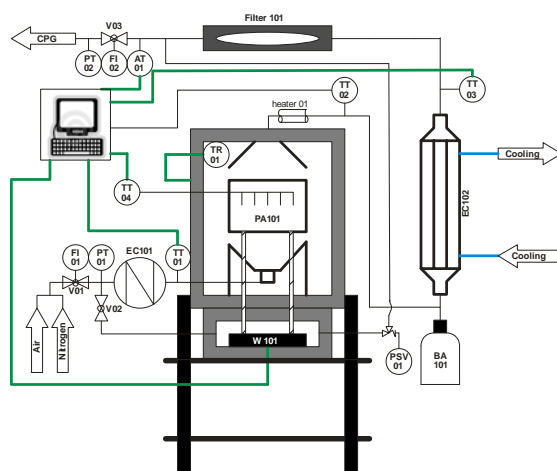


Figure 1 : Scheme of the high capacity thermobalance.

Process values (mass of the sample, flow rate of incoming nitrogen, flow rate of gas leaving the devices, temperatures) are recorded in the computer that supervises the overall device. Because of its tightness, this device allows verifying the overall mass balance of the operation with an error below 5% of the initial mass of the sample under investigation.

2.2- Mathematical model

Before entering the section devoted to the derivation of the mathematical model (state variables and associated equations) it is necessary to give insights on the system being studied.

2.2.1- System under study

In the frame of the study, the sample being processed is supposed to be composed of organic material, inorganic material (which becomes ash at the end of the thermal degradation), and of liquid water corresponding to the initial moisture content of the biomass. Because of the initial state of the biomass in the fixed bed (shredded particles gathered in a fixed bed), one is able to consider this bed as a two dimensional and porous one, filled with air saturated with water vapor at its initial temperature. The derivation of the mathematical model must then allow describing these four phases that might coexist (organic and inorganic material, liquid water and gas filling the pores of the bed and for which composition might be modified during the experiment).

Once drying of the sample is over, its temperature will rise again until it reaches a level at which the pyrolysis process will begin. A lot of work has been done in that context to predict the reaction pathway as well as the products of this operation (see for example [7-11]). It is commonly admitted that these products should be gathered in several categories:

- Solid fractions (intermediate and char)
- Tars (gaseous fraction that might be condensed at ambient temperature)
- Gas (Permanent gases).

The products of this first decomposition (primary pyrolysis) might undergo secondary reactions and processes (condensation and further evocation of the tars, chemical reactions between gases, (either condensable or permanent), heterogeneous reactions with char, that has also catalytic activity because of its ash content). Nevertheless, these secondary processes will not be taken into account within the frame of this study.

In order to take into account the whole set of phases and chemical species that might be produced during primary pyrolysis and in accordance with previous work that has been done in that context [5], the reaction pathway that has been considered is the one depicted On Figure 2.

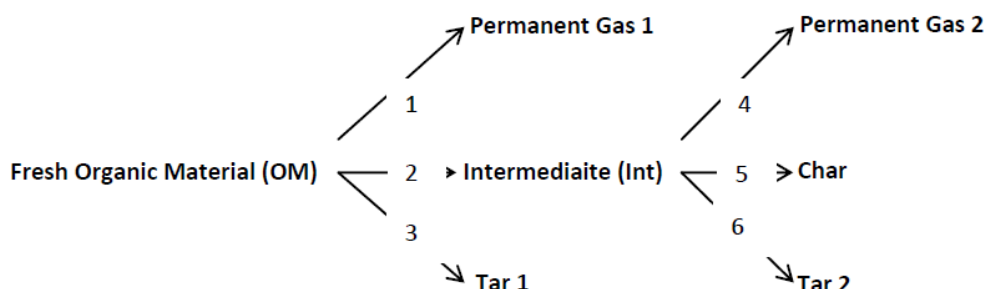


Figure 2: Reaction pathway taken into account in the model.

To sum up about the description of the system under study, it can be said that this one is composed of:

- Four different solid phases (organic and inorganic material, intermediate, char)
- Two liquid phases (free and bound water)
- A multicomponent gaseous phase, a part of which being condensable at ambient temperature.

Dealing with this last one, it is necessary to give information about the species that were considered to be present in the mixture. Accordingly to previous work [5] the following were taken into account: methane, hydrogen, carbon monoxide and dioxide, for the permanent species, and water, acetic acid, lactic acid, formic acid, hydroxyacetone, acetaldehyde, formaldehyde, methanol and furfural for the condensable ones. Finally, because of the presence of air in the sample at the beginning of the experiment, and because the sample is continuously swept by nitrogen during the process, oxygen and nitrogen were accounted for in the gaseous mixture.

2.2.2- State variables

In this section, the set of the different variables that will be computed by the model is presented. It comes as a support of the preceding paragraph. Each of these variables is a local one; its value depends upon the position where it is computed in the sample. The terms “phase average” and “intrinsic phase average”, referred to the formalism used in the context of volume averaging theory [3-4]. The set of the relevant variables is:

- $\langle T \rangle$ local phase average temperature of the sample (single value shared by the 7 phases at every location of the domain)
- $\langle P_g \rangle^g$ local intrinsic gas phase pressure.
- $\langle \rho_g \rangle^g$ local intrinsic density of the gas phase
- $\langle \rho_i \rangle^g$ local intrinsic mass concentration of species i in the gas phase (16 Species)

- $\langle \rho_l \rangle$ local average mass concentration of free water in the sample
- $\langle \rho_b \rangle$ local average mass concentration of bound water in the sample
- $\langle \rho_{OM} \rangle$ local average mass concentration of “fresh” organic material in the sample
- $\langle \rho_{INO} \rangle$ local average mass concentration of inorganic material in the sample
- $\langle \rho_{Int} \rangle$ local average mass concentration of intermediate in the sample
- $\langle \rho_C \rangle$ local average mass concentration of char in the sample
- ε_g local gaseous volume fraction

2.2.3- Main equations of the model

The main equations of the model are presented in this section. Because this is not the scope of the present work, their derivation is not presented here (derivations of the balance equations at the phase were continuum mechanics apply, subsequent averaging of these equations...). Instead, the choice has been made to show the equations required by the estimation of the variables presented in the preceding paragraph, highlighting the principle on which these equations rely on.

Balance on organic material

$$\frac{\partial}{\partial t} \langle \rho_{OM} \rangle = -k_1 \langle \rho_{OM} \rangle^{n_1} - k_2 \langle \rho_{OM} \rangle^{n_2} - k_3 \langle \rho_{OM} \rangle^{n_3} \quad (1)$$

Balance on intermediate

$$\frac{\partial}{\partial t} \langle \rho_{Int} \rangle = +k_2 \langle \rho_{OM} \rangle^{n_2} - k_4 \langle \rho_{Int} \rangle^{n_4} - k_5 \langle \rho_{Int} \rangle^{n_5} - k_6 \langle \rho_{Int} \rangle^{n_6} \quad (2)$$

Balance on inorganic material

$$\frac{\partial}{\partial t} \langle \rho_{INO} \rangle = 0 \quad (3)$$

Balance on char

$$\frac{\partial}{\partial t} \langle \rho_C \rangle = k_5 \langle \rho_{Int} \rangle^{n_5} \quad (4)$$

where $k_1, k_2, k_3, k_4, k_5, k_6, n_1, n_2, n_3, n_4, n_5$ et n_6 represent the reaction rate constants and orders associated to reaction 1, 2, 3, 4, 5 and 6 (Figure 2).

Balance on free water

$$\frac{\partial}{\partial t} \langle \rho_l \rangle + \frac{1}{r} \frac{\partial}{\partial r} (r \langle \rho_l \rangle' \langle v_l \rangle_r) + \frac{\partial}{\partial z} (\langle \rho_l \rangle' \langle v_l \rangle_z) = \langle \dot{w}_l \rangle \quad (5)$$

The transport terms involved in the preceding equation are computed as follows:

$$\langle v_l \rangle_r = - \frac{K_l K_l^r}{\mu_l} \frac{\partial}{\partial r} \langle P_l \rangle' \quad (6)$$

$$\langle v_l \rangle_z = - \frac{K_l K_l^r}{\mu_l} \frac{\partial}{\partial z} \langle P_l \rangle' \quad (7)$$

The « source term » $\langle \dot{w}_l \rangle$ corresponds to the evaporation or condensation of free water. The terms K_l and K_l^r stand respectively for the intrinsic and relative permeability of the media for the liquid phase while $\langle P_l \rangle'$ represents the local intrinsic pressure of the liquid phase which is computed according to:

$$\langle P_l \rangle' = \langle P_g \rangle^g - P_C \quad (8)$$

with P_C , the local capillary pressure.

Balance on bound water

$$\frac{\partial}{\partial t} \langle \rho_b \rangle + \frac{1}{r} \frac{\partial}{\partial r} (r \langle \rho_b v_b \rangle_r) + \frac{\partial}{\partial z} (\langle \rho_b v_b \rangle_z) = \langle \dot{w}_b \rangle \quad (9)$$

The transport terms involved in the preceding equation are computed as follows:

$$\langle \rho_b v_b \rangle_r = - \langle \rho_{SD} \rangle D_b \frac{\partial}{\partial r} \frac{\langle \rho_b \rangle}{\langle \rho_{SD} \rangle} \quad (10)$$

$$\langle \rho_b v_b \rangle_z = - \langle \rho_{SD} \rangle D_b \frac{\partial}{\partial z} \frac{\langle \rho_b \rangle}{\langle \rho_{SD} \rangle} \quad (11)$$

In the above expressions, $\langle \rho_{SD} \rangle$ stands for the average mass concentration of dry solid, while D_b represents the diffusion coefficient of bound water in the media. The « source term » $\langle \dot{w}_b \rangle$ corresponds to the evaporation or condensation of bound water.

The estimation of source terms involved in equations (5) and (9) is quite complicated; this is one of the reasons why these equations are summed up into a balance on liquid water:

$$\frac{\partial}{\partial t} (\langle \rho_b \rangle + \langle \rho_l \rangle) + \frac{1}{r} \frac{\partial}{\partial r} (r (\langle \rho_b v_b \rangle_r + \langle \rho_l v_l \rangle_r)) + \frac{\partial}{\partial z} (\langle \rho_b v_b \rangle_z + \langle \rho_l v_l \rangle_z) = \langle \dot{w}_b \rangle + \langle \dot{w}_l \rangle \quad (12)$$

and values of $\langle \rho_l \rangle$ and $\langle \rho_b \rangle$ are computed from the knowledge of the local value of $\langle \rho_b \rangle + \langle \rho_l \rangle$ according to relations involving the fibre saturation point.

Balance on gaseous species

$$\frac{\partial}{\partial t} (\varepsilon_g \langle \rho_i \rangle^g) + \frac{1}{r} \frac{\partial}{\partial r} (r \langle \rho_i v_i \rangle_r) + \frac{\partial}{\partial z} (\langle \rho_i v_i \rangle_z) = \langle \dot{w}_i \rangle \quad (13)$$

The transport terms involved in the preceding equation are computed using convection behavior under a pressure gradient and diffusion:

$$\langle \rho_i v_i \rangle_r = - \langle \rho_i \rangle^g \frac{K_g K_g^r}{\mu_g} \frac{\partial}{\partial r} \langle P_g \rangle^g - \langle \rho_g \rangle^g D_i \frac{\partial}{\partial r} \frac{\langle \rho_i \rangle^g}{\langle \rho_g \rangle^g} \quad (14)$$

$$\langle \rho_i v_i \rangle_z = - \langle \rho_i \rangle^g \frac{K_g K_g^r}{\mu_g} \frac{\partial}{\partial z} \langle P_g \rangle^g - \langle \rho_g \rangle^g D_i \frac{\partial}{\partial z} \frac{\langle \rho_i \rangle^g}{\langle \rho_g \rangle^g} \quad (15)$$

The terms K_g and K_g^r stand respectively for intrinsic and relative permeability of the media for the gaseous species. The source term occurring in equation (13) is evaluated according to the reaction pathway that was proposed on Figure 2:

$$\langle \dot{w}_i \rangle = \langle \dot{w}_i \rangle^{pyr} = k_1 Y_i^{perm,1} \langle \rho_{OM} \rangle^{n_1} + k_3 Y_i^{tar,1} \langle \rho_{OM} \rangle^{n_3} + k_4 Y_i^{perm,2} \langle \rho_{Int} \rangle^{n_4} + k_6 Y_i^{tar,2} \langle \rho_{Int} \rangle^{n_6} \quad (16)$$

where $k_1, k_3, k_4, k_6, n_1, n_3, n_4, n_6$ represent the reaction rate constants and orders associated to reactions 1,3, 4 et 6 while $Y_i^{perm,1}, Y_i^{perm,2}, Y_i^{tar,1}$ and $Y_i^{tar,2}$ stand respectively for the mass fractions of species i in the permanent gases 1 and 2 and in the tars 1 and 2.

The fate of gaseous water is a little different from the other gaseous species. Indeed, the source term must account for the generation of water by the reactions but also by condensation and/or evaporation of the liquid water:

$$\langle \dot{w}_{H_2O} \rangle = \langle \dot{w}_{H_2O} \rangle^{pyr} - \langle \dot{w}_l \rangle - \langle \dot{w}_b \rangle \quad (17)$$

Energy balance

$$\begin{aligned} & \frac{\partial (\varepsilon_g \langle \rho_g \rangle^g C_{p,g} + \langle \rho_l \rangle C_{p,l} + \langle \rho_b \rangle C_{p,b} + \langle \rho_{OM} \rangle C_{p,OM} + \langle \rho_{Int} \rangle C_{p,Int} + \langle \rho_{INO} \rangle C_{p,INO} + \langle \rho_C \rangle C_{p,C}) (T)}{\partial t} \\ & + \frac{1}{r} \frac{\partial}{\partial r} \left(r \left(\langle \rho_l \rangle^l \langle v_l \rangle_r C_{p,l} + \langle \rho_b v_b \rangle_r C_{p,b} + \langle \rho_g v_g \rangle_r C_{p,g} + \sum_{i=1}^{N_s} C_{p,g} \langle \rho_i U_i \rangle_r \right) (T) \right) \\ & + \frac{\partial}{\partial z} \left(\langle \rho_l \rangle^l \langle v_l \rangle_z C_{p,l} + \langle \rho_b v_b \rangle_z C_{p,b} + \langle \rho_g v_g \rangle_z C_{p,g} + \sum_{i=1}^{N_s} C_{p,g} \langle \rho_i U_i \rangle_z \right) (T) \\ & = \frac{1}{r} \frac{\partial}{\partial r} \left(r k_{eff} \frac{\partial}{\partial r} \langle T \rangle \right) + \frac{\partial}{\partial z} \left(k_{eff} \frac{\partial}{\partial z} \langle T \rangle \right) - \langle \dot{w}_{OM} \rangle \Delta h_{OM} - \langle \dot{w}_{Int} \rangle \Delta h_{Int} + \langle \dot{w}_{H_2O} \rangle^{vap} \Delta h_{vap} \end{aligned} \quad (18)$$

In the above expression, $k_{eff}, \Delta h_{OM}, \Delta h_{Int}$ et Δh_{vap} stand respectively for effective thermal conductivity of the media, and the heat of reactions associated to pyrolysis of “fresh” organic material, intermediate and vaporization of liquid water (that can also account for desorption heat of reaction in the case of bound water).

To this set of equations are associated algebraic equations which will not be presented here but which allow closing of the overall model. These last ones represent:

- Ideal Gas law
- Normalization of gas composition
- Distribution of liquid water into free and bound water
- Overall volume conservation
- Liquid-vapor equilibrium for pure water.

3- RESULTS AND DISCUSSION

3.1- Solving

The set of Partial Differential Equations (PDE's) and Algebraic one is firstly converted into an Ordinary Differential and Algebraic Equations (ODEA's) one according to the method of lines. More precisely, the finite volume method is used to convert the spatial and differential terms of the PDE's [12]. The "vertex centered" method has been used in this context. The resulting ODEA's set is solved according to the DASSL algorithm [13] using DisCO Software [14].

3.2- Operating conditions.

The sample which is considered here is pine, with a granulometry of the particles in the fixed bed of the order of magnitude of one millimeter. The basket of the sample is loaded with an initial mass of approximately 200g.

Once tightly closed, the device is fed with nitrogen at a flow rate of 15Nl/min. After 6 minutes of this sweeping procedure, the temperature of furnace (as well as the one of the nitrogen preheater EC101) is raised to 110°C. This value is kept during 60 minutes in order to ensure complete drying of the sample. Then, the relevant temperatures of the system (furnace and preheater) are further raised to 285°C with a heating rate of 20°C/min. This value is held during 5 minutes and then the powers to the furnace and to the preheater are switched off, and the natural cooling of the system proceeds. Figure 3 gives information on the operating conditions of the system.

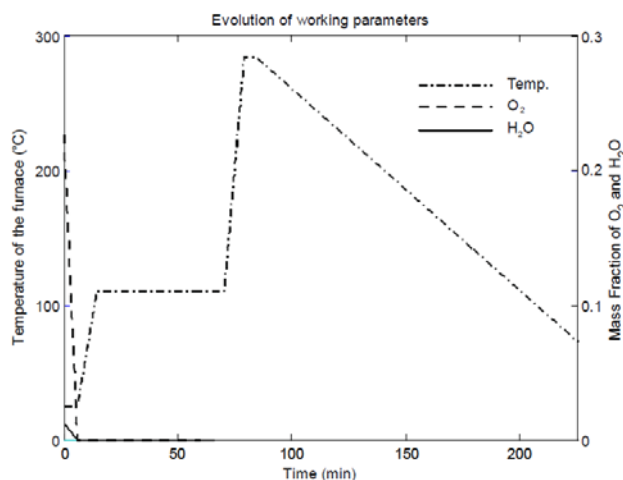


Figure 3: Operating conditions of the experiment under study.

3.3- Numerical parameters

To represent the above detailed operating conditions, the axisymmetric nature of the system has been taken into account. Hence, only a half of the basket has been simulated. 14 computational nodes have been used in both direction (height and radius). Given the 16 chemical species considered in the gas phase, the total number of equations that need to be solved by the time integrator is 5684 (22 ODE's and 7 AE's per computational nodes, on a mesh of 196 nodes). In order to avoid important computing time requirement during the correction part (of the "predictor-corrector algorithm used for time integration), which implies solving of a linear and algebraic set of equations, the sparse nature of the system has been taken into account. Indeed, only 127712 values of the convergence matrix are non-zero (the total size of the matrix is 32307856 elements) what justifies the use of linear space algebra to reduce the computing time. It has also to be noticed that this non-zero values were truly estimated (the derivative function of the equations were algebraically estimated instead of numerically with finite differences).

3.4- Validation

A complete validation of the model should imply that a comparison between the numerical and experimental transient and spatial profiles of temperature and composition within the sample be performed. Nevertheless, because of the measurement of the mass during the process, and because the presence of thermocouples or sampling devices would disturb this measurement, this information is not yet available. We will thus focus on a partial validation of the model where the predicted evolution of the mass of the sample is compared to the recorded one. This is the scope of Figure 4.

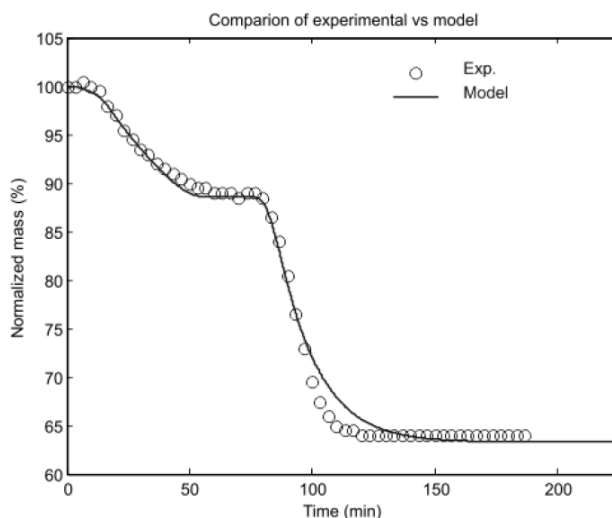


Figure 4: Transient evolution of the mass of the sample
Numerical vs experimental.

Given this comparison, one is able to remark that the drying of the sample is particularly well predicted by the model. Indeed, during this period, both the mass loss and the characteristic times match perfectly. Dealing with the pyrolysis step, the first period of the degradation is correctly estimated. However, one can also remark that the model under predicts the intensity of the phenomena at the end of the process, even though the final mass loss is correctly estimated. The above mentioned mismatch could be attributed to the value of the effective thermal conductivity that has been entered in the model as a constant and that do not take into account the evolution of this data with the evolution of the composition of the sample.

3.5- Further analysis of the results

One important feature of the model is that it provides internal profiles of temperature and composition of the sample as it is being processed. As an illustration, Figures 5 and 6 respectively show the evolution of the temperature of the sample and of the mass concentration of the “fresh” organic material as they are computed by the model.

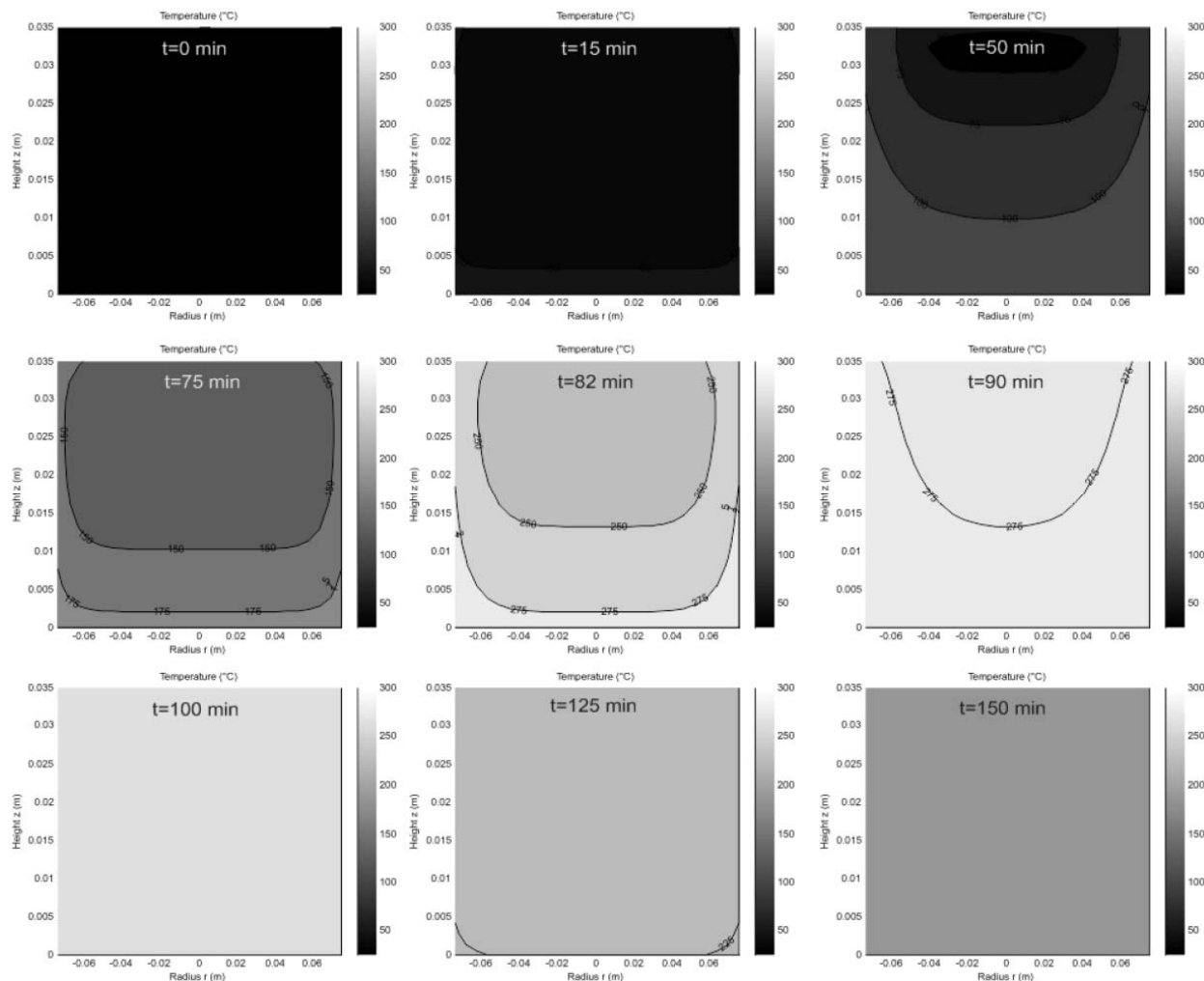


Figure 5: Numerical profiles of the temperature of the sample.

The analysis of these figure shows that, as the drying step is not finished yet, the temperature of the sample does not raise and stay below the temperature of the furnace (Such an assertion could be confirmed by the profile of moisture content within the sample which shows that the complete drying of the sample is done after 70 minutes). Once this drying step is over, the temperature of the sample raises, at its bottom at the beginning (under the effect of hot nitrogen supply), and to a lower extent, by its walls. Given this local increase in the temperature level, the thermal degradation of the organic material proceeds and its evolution is in accordance with the evolution of the temperature within the sample.

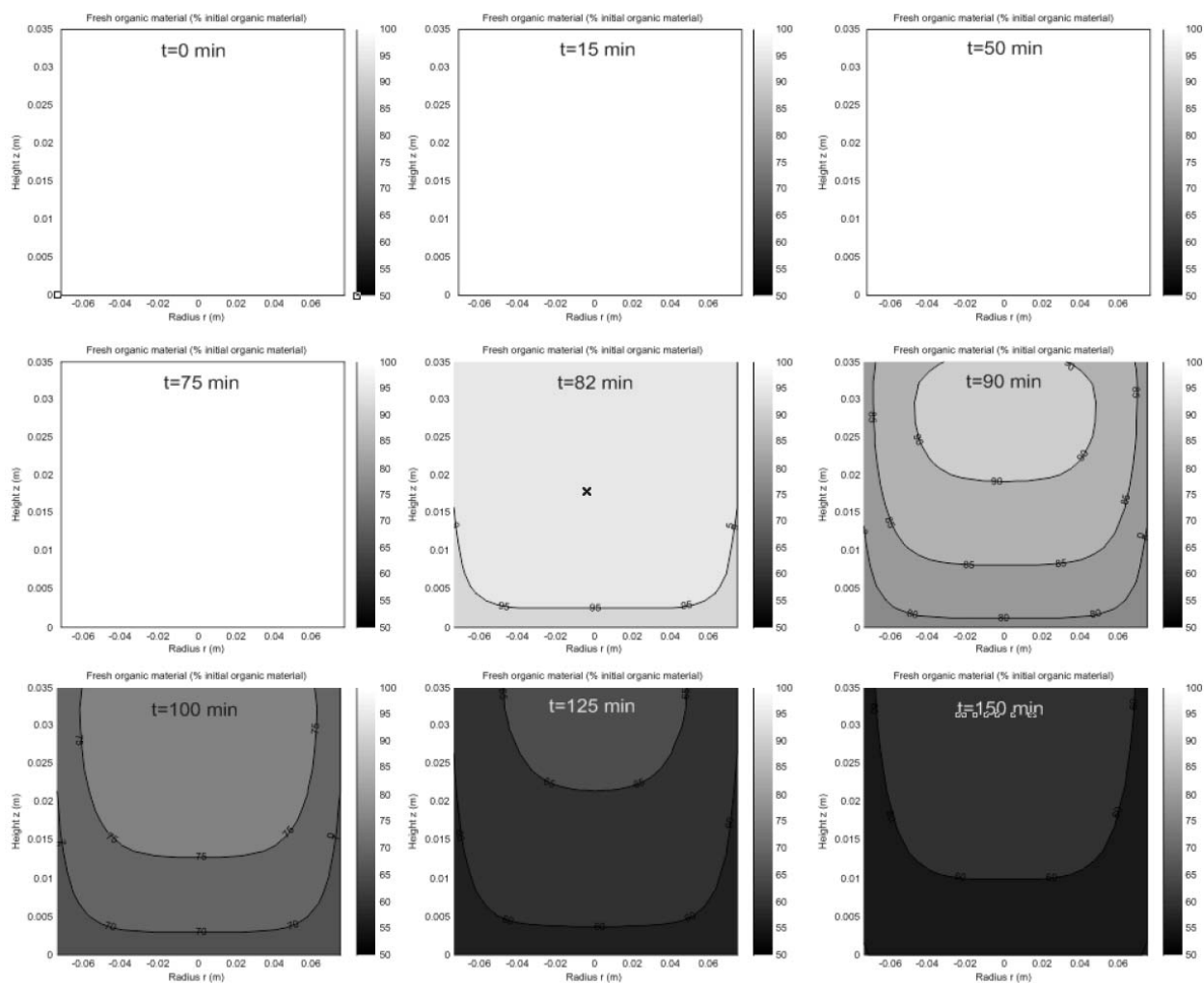


Figure 6: Numerical profiles of mass concentration of “fresh” organic material within the sample.

4- CONCLUSION

This article has given a presentation of the first step of a more consequent work. Up to now, a mathematical model has been derived. It represents the relevant phenomena occurring within a fixed bed undergoing slow drying and pyrolysis processes. This model, which relies on the volume averaging theory, has been partially validated by comparison of its results with results obtained in a high capacity thermobalance. This first step requires further validation by comparison of internal profiles of temperature for example.

Once this supplementary validation has been performed, the coupling between both tools (high capacity thermobalance and numerical model) will be used to give insights and information on the reaction pathway (as well as the associated kinetics) involved during slow pyrolysis of organic resources. This information will take the form of the reaction rate for solid degradation, but also for gaseous chemical species production, which is an information rarely given in the literature.

5- ACKNOWLEDGMENTS

The authors would like to thank the “Pôle de Calcul Scientifique et de Traitement de Données de l’Université de Pau et des Pays de l’Adour” for its assistance in the use of computing resources required by this study.

REFERENCES

- [1] R.C. Brown, “*Thermochemical Processing of Biomass*”, 2011, John Wiley & Sons.
- [2] E. Hogan, J. Robert, G. Grassi, A.V. Bridgwater, “*Biomass Thermal Processing*”, 1992, CPL Press.
- [3] Whitaker, S. Simultaneous heat, mass, and momentum transfer in porous media: a theory of drying, *Advances in Heat Transfer*, 1977, 13 : 119-203.
- [4] Quintard, M. ,Whitaker, S. 1996, Transport in Chemically and Mechanically Heterogeneous Porous Media I: Theoretical Development of Region Averaged Equations for Slightly Compressible Single-Phase Flow, *Advances in Water Resources* **19**(1), 29-47
- [5] Casajus C., *Torréfaction de biomasses lignocellulosiques*. PhD. Thesis Université de Pau et des pays de l’Adour, 2010.
- [6] Marias F., Casajus C. Torrefaction of corn stover in a macro thermobalance. Influence of Operating conditions. *Waste and Biomass Valorisation*, (**5**) 157-164, 2014.
- [7] Shafizadeh F., Chin P.S., Thermal deterioration of wood, *Wood technology: Chemical Aspects, ACS Symp. Ser.*, 1977, (**43**), 57-81
- [8] Thurner F., Mann U., Kinetic investigation of wood pyrolysis, *Industrial Engineering Chemistry Process Design and Development*, 1981, (**20**), 482-488.
- [9] Orfão J.J.M., Antunes F.J.A., Figueiredo J.L. Pyrolysis kinetics of lignocellulosic materials--three independent reactions model. *Fuel* ,1999, (**78**), 349-358.
- [10] Di Blasi C., Lanzetta M., Intrinsic kinetics of isothermal xylan degradation in inert atmosphere. *Journal of Analytical and Applied Pyrolysis*, 1997 (**41**), 287-303.
- [11] Koufopoulos C.A., Mashio G., Kinetic modelling of the pyrolysis of biomass and biomass component. *The canadian journal of chemical engineering*, 1989 (**67**), 75-84.
- [12] Patankar S.V., *Numerical Heat Transfer and Fluid Flow*, Hemisphere Publishing Corporation, Washington, DC, 1980.
- [13] Ascher U.M., Petzold L.R. , *Computer methods for ordinary differential equations and Differential Algebraic equations*, SIAM, 1998..
- [14] Sargousse A., Le Lann J.M., Joulia X., and Jourda L., Disco, *un nouvel environnement de simulation orientée objet*, In MOSIM’99, Modélisation et simulation des flux physiques et informationnels, 2ème Conférence Francophone de Modélisation et Simulation, Annecy, 1999.